
AtomSurf: Surface Representation for Learning on Protein Structures

Vincent Mallet^{*1} Souhaib Attaiki^{*1} Maks Ovsjanikov¹

Abstract

An essential aspect of learning from protein structures is the choice of their representation as a geometric object (be it a grid, graph, or surface), which conditions the associated learning method. The performance of a given approach will then depend on both the representation and its corresponding learning model. In this paper, we investigate representing proteins as *surfaces embedded in 3D* and evaluate this representation within an established benchmark (Townshend et al., 2020). Our first finding is that despite promising results, state-of-the-art surface-based learning approaches alone are not competitive with other modalities on this benchmark. Building on this, we introduce a novel synergistic approach that incorporates graph and surface-based approaches within a single learnable architecture. We show that using this combination, which inherits the strengths of the two representations, we obtain state-of-the-art results across *all tested tasks*, on the Atom3d benchmark, as well as on binding pocket classification. Our code and data can be found online: <https://github.com/Vincentx15/atom2D>.

1. Introduction

Structural bioinformatics data is becoming available at an unprecedented pace. Advances in cryogenic Electron Microscopy (cryo-EM) in particular, have led to the production of evermore experimentally derived structures, as well as larger systems and better resolutions (Fontana et al., 2022). The development of AlphaFold (Jumper et al., 2021) along with many subsequent works have made protein structures abundantly available, with more than a million high-quality predictions included in the Protein Data Bank (PDB) (Berman, 2000) and over 600 million in the ESM Metagenomic Atlas (ESMatlas) (Lin et al., 2022). There is thus a growing demand for machine learning techniques, which

can leverage this structural data to help advance the fields of structural bioinformatics and drug design.

Protein structures are complex objects characterized both by atomic coordinates as well as intricate bio-chemical interactions between them. They also exhibit *geometric* properties as objects in 3D space, including, e.g., the absence of a canonical orientation due to the insignificance of gravity at atomic scales. Moreover, proteins have a hierarchical structure with atoms organized in larger building blocks, the amino acids, enabling the use of coarser encodings.

To be used in a learning pipeline, an initial modeling step transforming protein structures into a well-defined mathematical object is necessary. Several representations have emerged, focusing on different aspects of protein structures. The sequence representation completely disregards the geometric nature of protein structures, but enables training on large data sets, yielding impressive performance (Rao et al., 2021), especially considering the complete lack of geometric information in this encoding. The point cloud representation disregards the connectivity induced by chemical interactions, but allows for the most generic geometric description of the data. The graph representation does the opposite by keeping only the chemical connectivity and discarding the atomic positions. Geometric graphs (Duval et al., 2023) keep both information by including the atomic positions in the graph nodes, opening the door to graph message passing accounting for edge geometry. Finally, protein *surfaces* choose to trade fine-grained information of the interior of a protein for an accurate depiction of its outer surface, enabling computation of curvatures and geodesics. This representation is thought to be of particular interest to study active interaction sites that mostly depend on properties of the surface because of the screening effect. However, even for those interactions dominated by surface terms, knowledge of the interior can encode the stability of the surface. These different representations are illustrated in Figure 1.

The choice of representation is particularly prominent in the context of *learning-based* methods, as specialized architectures have been developed to process each type of data. The range of approaches is studied within the field of geometric deep learning (Bronstein et al., 2017), and specialized methods have been developed to process different data types from graphs (Bruna et al., 2013; Kipf & Welling,

^{*}Equal contribution ¹LIX, Ecole Polytechnique, IPP Paris. Correspondence to: Maks Ovsjanikov <maks@lix.polytechnique.fr>.

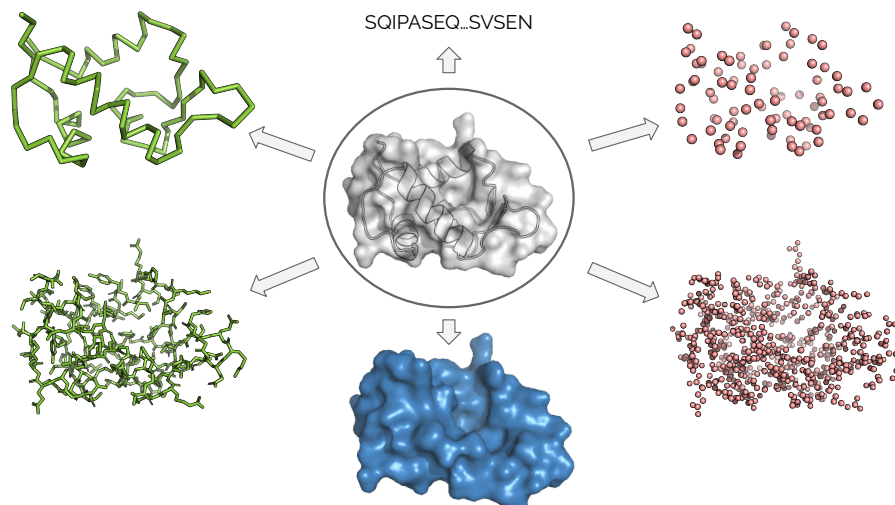


Figure 1: This figure illustrates the diverse mathematical objects used to represent a protein structure, ranging from sequences and molecular surfaces (blue) to atom-level and residue-level point clouds (red) and graphs (green). Effective machine learning for protein structures hinges on selecting the appropriate mathematical representation, followed by a compatible machine-learning technique. This dual-layered modeling approach underscores the complexity of extrapolating performance solely based on machine learning benchmarks in protein structure tasks.

2016), to point clouds (Qi et al., 2017; Wang et al., 2019), surfaces (Masci et al., 2015; Monti et al., 2017), *equivariant* methods that respect a group symmetry of the data (Cohen & Welling, 2016a;b), and more.

A few pioneering works have applied geometric deep learning to structural biology data representations, using 3D convolutional networks (Jiménez et al., 2017), equivariant convolutional networks (Weiler et al., 2018), surfaces (Gainza et al., 2020a), graphs (Aumentado-Armstrong, 2018) and equivariant discrete networks (Stärk et al., 2022). They were followed by several others, especially in the post-AlphaFold era and we refer the reader to (Isert et al., 2023) for a review of different methods. At the core of this endeavor lies a dual challenge: selecting a suitable mathematical representation of protein structures and devising an effective learning method compatible with the chosen representation. Although benchmarking learning methods is relatively straightforward, the optimal modeling choice, involving the underlying representation and the associated learning method remains an open problem.

The seminal work of Atom3d (Townshend et al., 2020) aims to address this question by proposing a set of nine benchmark tasks for three-dimensional molecular structures. The authors also compare different representations by evaluating neural networks based on 3D grids, graphs, and equivariant networks on the proposed tasks.

This comparison does not, however, include the surface representation, despite promising results (Gainza et al., 2020a;

Sverrisson et al., 2021). At the same time, these results were achieved using one of the earliest surface-based learning architectures (Masci et al., 2015) and a relatively ad-hoc method. More recent surface-based approaches, such as *DiffusionNet* (Sharp et al., 2022), are now well established. A concurrent work has recently applied this method to protein data (Wang et al., 2023). However, approaches based on the surface representation have followed the initial MaSIF paper validation (Gainza et al., 2020b), and hence *have never been directly compared to other representations* in the context of a single well-established benchmark.

Beyond using a single representation for proteins, several papers have relied on the flexibility of the graph representation to incorporate information from several modalities simultaneously. In (Hermosilla et al., 2020) the authors enrich the graph with additional edge types that encode the sequence. In (Somnath et al., 2021) the representation is instead enriched with a graph encoding of a surface mesh, along with edges connecting graph nodes and mesh vertices. However, relying on graph neural networks instead of surface-based methods in such a scenario is potentially limiting, as it can both lead to sensitivity to the exact mesh topology and impede long distance communication due to over-smoothing (Li et al., 2018; Sharp et al., 2022).

In our study, we rigorously evaluate the performance of surface-based methods by applying *DiffusionNet* to the Atom3d benchmark, offering *the first direct and fair comparison* of the surface representation against other repre-

sentations and introducing a batched implementation of *DiffusionNet* along the way.

In addition, we also propose a novel learning-based method tailored to protein data, by combining the surface and graph-based representations within a single architecture. Our approach incorporates information about both the internal intricate structure of the protein, encoded by the graph and the geometric properties of the surface, each processed with the appropriate learnable model. We observe that the learning-based frameworks on these two representations are complementary: one allows local message passing, whereas the other one enables global communication via learned diffusion. Our unified approach thus inherits these strengths and, as we demonstrate below, leads to state-of-the-art results on all tasks in (Townshend et al., 2020), as well as on binding pocket classification.

2. Methods

In this section, we describe the methodology behind our work. In Section 2.1, we discuss the approach we adopt for modeling proteins as graphs. In Section 2.2, we present the technique for creating 3D surface mesh models of protein data and the specialized deep neural network architecture developed for processing these models. Section 2.3 highlights a challenge associated with directly employing the surface-based network, which empirically leads to sub-optimal results, and presents solutions to mitigate these issues. In Section 2.4, we propose a novel hybrid representation, which synergistically integrates graph and surface information within a unified architecture, optimizing the performance by leveraging the advantages of both representations. Lastly, in Section 2.5, we provide the details regarding the chosen architecture to take advantage of this dual representation.

2.1. Graph Representation Learning

For a given protein, denoted by \mathbf{P} , we construct a graph representation $\mathcal{G} = (\mathcal{V}_g, \mathcal{E}_g)$. To ensure consistency and fairness in comparison, we follow the conventions established by *Atom3d* (Townshend et al., 2020). In this framework, each node in the graph corresponds to an atom within the protein. Edges \mathcal{E}_g are defined between pairs of atoms that are within a 4.5 angstrom radius cutoff, considering them as neighbors. Initial features for each node are encoded using one-hot vectors that represent atom types.

The graph encoder we employ aligns with the architecture described in *Atom3d*. Specifically, it consists of a sequence of five layers, where each layer is a combination of Graph Convolutional Networks (GCN) as proposed by Kipf and Welling (Kipf & Welling, 2016), interspersed with Batch Normalization operations.

2.2. Surface Representation Learning

To generate the surface representation $\mathcal{S}_{\mathbf{P}}$ of the protein \mathbf{P} , our initial step involves computing the protein surface using MSMS (Sanner et al., 1996). This process begins with the default vertex density, which is incrementally increased until we achieve a minimum threshold of 128 vertices. Subsequently, to manage the size of the largest meshes obtained through this method, we employ quadratic decimation (Garland & Heckbert, 1997), effectively reducing their complexity.

Once we have the optimized triangular mesh $\mathcal{S}_{\mathbf{P}}$, consisting of n vertices, we construct the cotangent Laplace-Beltrami operator Δ_S (Meyer et al., 2003; Vallet & Levy, 2008), which encodes the surface’s intrinsic geometry. We extract $k = 128$ smallest eigenvalues of Δ_S and organize them in a diagonal matrix $\Lambda \in \mathbb{R}^{k \times k}$, along with the corresponding eigenvectors stacked within the matrix $\Phi \in \mathbb{R}^{n \times k}$. Additionally, a diagonal matrix of area weights, $M \in \mathbb{R}^{n \times n}$, is defined.

As the basis for our surface-based learning method, we employ the *DiffusionNet* approach, presented in (Sharp et al., 2022). This method has been proven highly effective across a diverse set of tasks, including classification, segmentation, and shape matching, notably due to its robustness and its ability to perform long range and multi-scale information propagation.

The mathematical foundation of *DiffusionNet* is the heat equation, which simulates the diffusion of heat, or, equivalently, the behavior of Brownian motion on a surface over time. This process is described for a surface S with a function $\mathbf{f} : S \rightarrow \mathbb{R}$ that defines the initial state of diffusion. The equation governing this diffusion process is as follows:

$$\frac{\partial \mathbf{f}}{\partial t} = \Delta_S \mathbf{f}, \quad (1)$$

where $\frac{\partial \mathbf{f}}{\partial t}$ represents the rate of change of \mathbf{f} over time.

DiffusionNet constructs a neural network architecture by emulating the heat equation’s effects on the surface and making the time a *learnable* parameter. Specifically, within *DiffusionNet*, a *diffusion layer* at a given learned time t , denoted as \mathbf{h}_t , is defined by the equation:

$$\mathbf{h}_t(u) := \Phi e^{-\Lambda t} (\Phi^T M) u, \quad (2)$$

where u signifies the input feature set at time t . This mechanism relies on dense linear algebra operations, such as element-wise exponentiation and matrix multiplication, offering straightforward differentiation with respect to both u and t . In (Sharp et al., 2022), the diffusion layers are combined with features based on function gradients and standard MLPs. This leads to an architecture that enables signal propagation across the surface, which can capture the surface’s geometric nuances in a task-specific manner.

To establish a benchmark method for surface analysis on `Atom3d`, we utilize three *DiffusionNet* blocks, applying them to the protein surfaces \mathcal{S}_P under consideration.

2.3. Adapting to Protein Surfaces of Diverse Scales

Applying the *DiffusionNet* architecture directly to protein datasets, without modifications, yields suboptimal performance. This discrepancy arises from the necessity to account for the intrinsic *scale* of proteins for accurate predictive modeling, a factor not considered in *DiffusionNet*’s original evaluations, which normalized all shapes to a uniform surface area. Tasks such as ligand-binding preference determination critically depend on the relative sizes of proteins and ligands, making scale considerations essential.

The efficacy of *DiffusionNet*’s receptive field is contingent upon the diffusion times learned within each diffusion layer. However, variations in the scale of input shapes can lead to discrepancies in the network’s learned receptive field. This is elucidated by the following proposition, with a proof provided in the supplementary material:

Proposition 2.1. *Let X be a shape and $Y = \alpha X$ its scaled version by a factor $\alpha > 0$. Denoting by $E.(t, x)$ the expected geodesic distance for a Brownian motion starting from point x after time t , it holds that:*

$$E_Y(t, x) = \alpha E_X\left(\frac{t}{\alpha^2}, x\right).$$

Importantly, note that the *time-parameter* of diffusion must be adapted depending on the scale, whereas in *DiffusionNet* the learned time parameters are shape independent. This relationship indicates that, in general, the expected geodesic distance—and by extension, the receptive field of the diffusion process—differs for shapes of varying scales, despite being identical in form. The diversity in size among protein datasets leads to instability during training. This instability complicates the model’s ability to learn effectively, posing challenges for achieving convergence.

To address this issue, we enhance the original *DiffusionNet* framework in two ways. First, we enable support for batch sizes greater than one (the original model was limited to batch sizes of one) and incorporate a Batch Normalization layer (Ioffe & Szegedy, 2015) after each diffusion layer. These modifications mitigate the instabilities in the training process.

Secondly, we noted that the learned diffusion times were initially set to zero in the original implementation. To address the challenge of scale variation, we facilitated the optimization process by incorporating biological priors relevant to spatial scales. Consequently, we determined that diffusion times approximating 2 resulted in receptive fields around 5 Å, which aligns with the spatial scale of binding sites.

Inspired by the inherent multi-scale nature of protein structures, we opted to draw samples from a normal distribution $t \sim \mathcal{N}(2, 2)$, characterized by a relatively high variance. The absolute values of these samples were then utilized as the initial values for our diffusion timescales.

Empirical evidence suggests that these adjustments significantly improve the network’s stability issues and allow it to converge (see Figure 5). In addition, these changes enable it to achieve comparable performance to other representations, as detailed in Section 3. Our enhanced *DiffusionNet* implementation is accessible in the provided code repository.

2.4. Hybrid Representation Learning

As mentioned earlier, different representations offer unique advantages and disadvantages. Surface representations capture the intricate geometric details critical for tasks involving protein interactions, while graph representations detail the atomic interactions within a protein’s interior that indirectly influence its surface dynamics and interaction capabilities. Furthermore, these representations facilitate complementary approaches to learning: local message passing through graphs and global information dissemination for surfaces via learned diffusion in (Sharp et al., 2022).

Therefore, beyond assessing the efficacy of surface and graph representations individually, we explore the benefits of integrating these representations in a unified framework. This integration aims to harness the distinct strengths of each representation to achieve improvements in performance.

To construct our hybrid approach, we start by building a bipartite graph $G = (\mathcal{V}, E)$, where $\mathcal{V} = \mathcal{V}_g \cup \mathcal{V}_s$ represents graph nodes and surface vertices, respectively. We compute geometric distances between nodes across these sets, forming edges in the bipartite graph when distances are below a specific threshold. This threshold is crucial: too restrictive, and the graph may become fragmented; too lenient, and it might resemble a biclique. An optimal threshold identified at 8 Å facilitates the formation of appropriate neighborhoods. Distance metrics may also be incorporated as edge attributes.

We now define block operations that can be stacked, and let i denote the index of the current block. In our framework, encoders on surfaces and graphs are denoted as f_θ^i and g_θ^i , respectively. We denote the input features on our hybrid representation as $\mathcal{X} = \mathcal{X}_g \cup \mathcal{X}_s$ and the set of input features to the i -th block as $\mathcal{X}^i = \{x_n^i, n \in \mathcal{V}\}$. The corresponding encoded features are thus $\mathcal{H}^i = \{h_n^i, n \in \mathcal{V}\}$ with $h_n^i = f_\theta^i(x_n^i)$ for nodes $n \in \mathcal{V}_s$ and $h_n^i = g_\theta^i(x_n^i)$ for nodes $n \in \mathcal{V}_g$.

Our general methodology incorporates message-passing neural networks, denoted MP_θ^i , over the bipartite graph, such that $\mathcal{X}^{i+1} = \text{MP}_\theta^i(\mathcal{H}^i)$. By employing distinct sets,

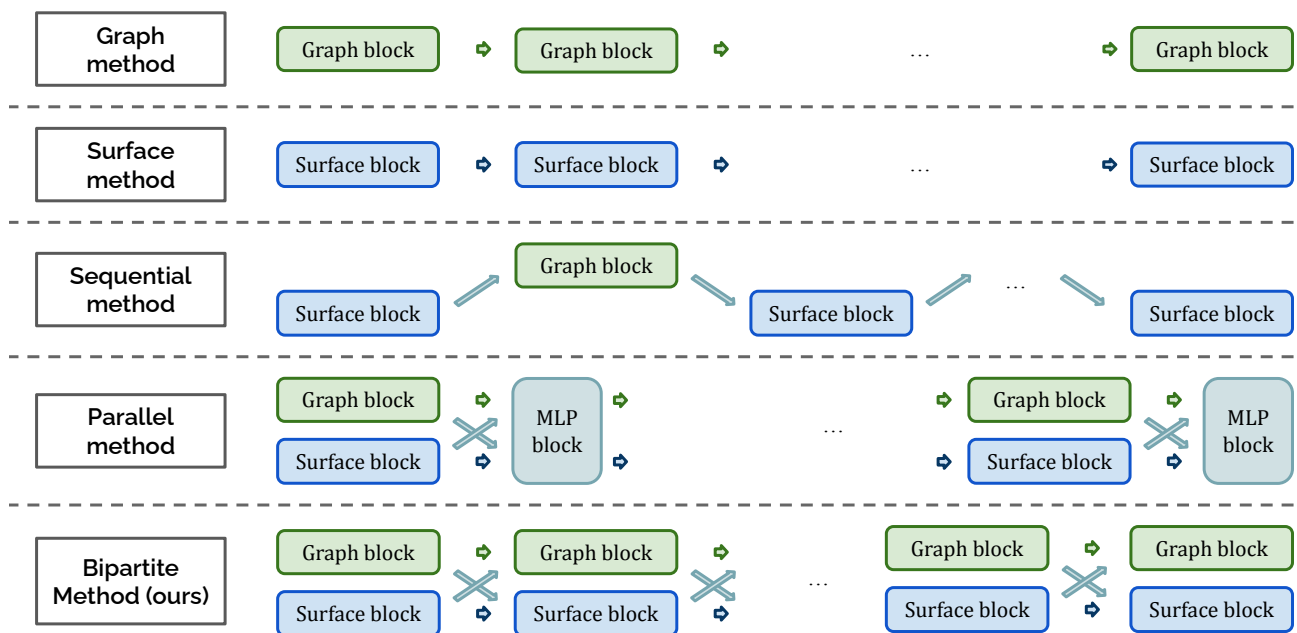


Figure 2: Different ways to leverage surface and graph information.

θ_{sg}^i and θ_{gs}^i , the architecture handles messages traversing from the surface to the graph and vice versa. In what follows, we drop the i superscript for simplicity and assume we are at a certain layer of the graph.

2.5. Proposed architecture

Our framework incorporates surface encoding blocks, f_θ^i , which consist of a diffusion operation followed by a point-wise neural network with two hidden layers of a specified width. Similarly, our graph encoding blocks, g_θ^i , are comprised of Graph Convolutional Networks (GCN) with a single hidden layer of a predetermined width. In our experiments, the widths for both encoding blocks were consistently set to equal values.

Exploring different strategies for combining surface and graph blocks yields various hybrid architectures, illustrated in Figure 2.

Our initial attempt involves a sequential alternation between surface and graph encoding, referred to as the *sequential* setting. This approach involves a two-step block: first, surface encoding is performed and its features are projected onto the graph via message passing, denoted as $h_n^g = \text{MP}_{sg}(f_\theta(\mathcal{X}))(n)$. This process generates intermediate graph node embeddings, represented as $\mathcal{H}^g = \{h_n^g, n \in \mathcal{V}_g\}$. Subsequently, these node embeddings are propagated within the graph to derive surface embeddings again, using $\mathcal{X}_{out} = \text{MP}_{gs}(g_\theta(\mathcal{H}^g))$. The architecture proposed by (Somnath et al., 2021) fits within this sequential framework, employing just one block and sum pooling

for message passing.

However, the sequential approach does not simultaneously leverage the distinct scales (local and global) offered by graph and surface processing. To overcome this, the *parallel* approach processes graph and surface features concurrently in separate encoders. Following this parallel processing, message passing is executed in both directions, and the outcomes are concatenated with the original encoded features. This process is formalized as $x_n = \text{MLP}(h_n \parallel \text{MP}(\mathcal{H})(n))$, where a Multi-Layer Perceptron (MLP) acts on the results of the concatenation.

Although flexible, this approach allocates learnable parameters to MLPs applied to the aggregated results of the message passing. While essential for models with unparameterized message passing (e.g., mean pooling), these parameters have a lesser impact compared to incorporating learnable parameters directly into the message-passing process. Consequently, we introduce the *bipartite* model, based on the equation:

$$x_n = \alpha h_n + \text{MP}_{gs}(\mathcal{H})(n) + \text{MP}_{sg}(\mathcal{H})(n), \quad (3)$$

where $\alpha \in \mathbb{R}$ is set to $\alpha = 1$, and the message-passing utilizes a Graph Attention Layer (Veličković et al., 2017) with learnable parameters.

We evaluate these three configurations and conduct several ablation studies on our final model, discussed in Section 3.5.2. Finally, we provide the implementation details in Appendix A.

3. Results

3.1. Experimental Setup

We first start our validation by using the `Atom3d` benchmark, focusing on its three tasks exclusive to proteins. We now briefly introduce these three tasks :

Protein Interaction Prediction (PIP) : This task aims to predict which part of a protein interacts with which part of another. Framed as a classification task, pairs of residues from two proteins are labeled as positives if they interact and as negatives if they do not. The dataset comprises 87k, 31k, and 15k training, validation, and test examples.

Mutation Stability Prediction (MSP) : The objective here is to determine if a mutation enhances the stability of protein-protein interaction. Given a protein-protein interaction structure and its mutated version, this classification task labels the pair as a positive example if it exhibits increased stability. This task includes 2864, 937, and 347 examples in each data split. For both PIP and MSP, the performance metric is the Area under the Receiver Operating Characteristic curve (AuROC).

Protein Structure Ranking (PSR) : PSR is a regression task and aims to assign a quality score to predicted protein structures from the Critical Assessment of Methods of Protein Structure Prediction (CASP) (Kryshtafovych et al., 2019) competition. The PSR data train, validation, and test splits hold 25.4k, 2.8k, and 16k systems respectively. The "global R_S " term represents the mean correlation across all systems and proposals. Meanwhile, "mean R_S " refers to the average correlation for each system.

In addition to the `Atom3d` benchmark tasks, we evaluate our proposed approach on the task of ligand-binding preference prediction for protein binding sites, introduced as **Masif-ligand** in (Gainza et al., 2020b). Binding sites are regions of protein surfaces where small molecules (ligands) interact with the protein. A fine characterization of those regions helps understanding protein functions and plays a significant role in drug design and discovery. This dataset consists of protein binding sites that accommodate one of seven co-factors. It comprises 1,634 training instances, 202 validation instances, and 418 test cases. Given a binding site, the task amounts to predicting its corresponding co-factor.

3.2. Performance of Surface Representation

Our initial training is focused on a surface-centric approach. For the sake of fairness, we only use atom types as input and keep the same number of parameters as other methods of the `Atom3d` benchmark. We expect the surface representation to mostly perform well on tasks relative to interactions, and to underperform on the PSR task that also pertains to subtle

changes inside the protein volume with no impact on the protein surface. We present the results in Table 1.

		3DCNN	Graph	ENN	Surface
PIP	AuROC	0.844	0.669	-	0.837
MSP	AuROC	0.574	0.609	0.574	0.5
PSR	local R	0.431	0.411	-	0.330
	global R	0.789	0.750	-	0.643

Table 1: Comparison of different representations, including surface performance. The dashes in the equivariant methods' column refer to the impossibility to use the method because of memory constraints.

Surprisingly, we observe that the surface method consistently falls short in its performance, even on the protein-protein interaction task. Such an observation challenges assertions in previous purely surface-based methods, and highlights the importance of direct benchmarking in general. Despite promising modeling of protein interfaces, which are intrinsically surface objects, the network's training was unstable and could not reach satisfactory test performance. We emphasize that all networks are trained in a vanilla setting, in particular, unlike `MaSIF`, our input features are minimalistic. Perhaps surface networks shine when supplemented with richer information. However, when all input features are equal, surface networks are not top performers.

3.3. Synergy in Combined Representations

In this section, we assess the performance of our proposed method, which has the particularity of combining surface and graph representations. We use the same experimental setup and compare the use of previous state-of-the-art (SOTA) to models exclusively grounded in graphs or surfaces, and to ours. The results are presented in Table 2.

		SOTA	Graph	Surface	Ours
PIP	AuROC	0.844	0.669	0.837	0.876
MSP	AuROC	0.609	0.609	0.5	0.707
PSR	local R	0.432	0.411	0.330	0.452
	global R	0.796	0.750	0.643	0.831

Table 2: Comparison of our proposed approach with methods relying only on graphs or surfaces and with state-of-the-art (SOTA). Our method improves current best performance on all tasks.

Our method outperforms the state-of-the-art in all three tasks. Interestingly, its results surpass both graph-only and surface-only strategies, hinting at a synergy between the two representations. Achieving this is noteworthy because, to

maintain a consistent parameter count, both the graph and surface encoders are considerably condensed. An interesting result is that even in the case of PSR, where the use of surfaces does not intuitively seem relevant, the mixed model outperforms its graph counterpart with a comfortable margin. One possible interpretation for this result is *DiffusionNet*’s ability to perform long-range message passing.

3.4. Evaluation of Binding Sites Classification

This subsection is dedicated to evaluating the effectiveness of our methods in the binding sites classification task. We benchmark our approach against two recent methods: MaSIF (Gainza et al., 2020a) and HMR (Wang et al., 2023), with the latter being recognized as the state-of-the-art in this domain. To ensure a fair comparison, we employ a similar set of input features as these baselines, including hydrophobicity score and partial charge for chemical features, as well as mean/Gaussian curvature and Heat Kernel Signatures (Sun et al., 2009) for geometric features. Additionally, we fine-tune the hyperparameters of our architecture—specifically depth and width—to match the parameter count of HMR. Consistent with prior studies, we use balanced accuracy (the average recall achieved for each class) as our performance metric.

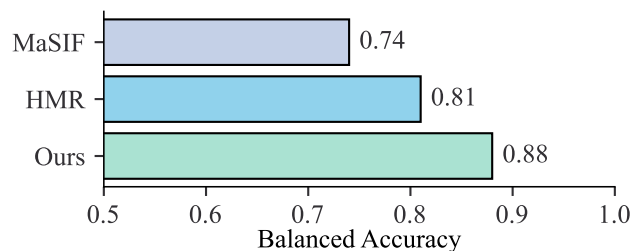


Figure 3: Balanced accuracy of binding sites classification.

As depicted in Figure 3, our method surpasses the benchmark methods and sets a new state-of-the-art for this task. Unlike HMR, which relies solely on surface representation, our results further validate the efficacy of synergistically combining surface and graph representations, showcasing that this integration leads to superior performance in ligand-binding pocket classification.

3.5. Further Analysis

3.5.1. QUALITATIVE RESULTS

To visualize our PIP model’s predictions, we aim to display patches of probability across the protein surface. The challenge is that the PIP task operates over pairs of residues in the graph and does not inherently provide a global interactability score for individual residues. Given a pair of protein chains A and B, assume, without loss of gen-

erality, that we want to plot the interaction site of protein B. We retrieve the nodes in protein A that belong to at least one positive pair and call the sets of such nodes \mathcal{N}_A^p . We define the interactability score of a node $I(n)$ as the indicator function of this set over graph nodes. We compute our model predicted probability \hat{p} on all pairs and get $\hat{p}(n_1, n_2) \in \mathcal{N}_A^p \times \mathcal{N}_B$ and get a set of predictions. The final predicted interactability \hat{I} of our model for a node $n_b \in \mathcal{N}_B$ is given as $\hat{I}(n_b) = \max_{n_a \in \mathcal{N}_A^p} \hat{p}(n_a, n_b)$.

For a visually appealing representation of the protein surface, we employ a straightforward message-passing (MP) mechanism without convolution on our standard bipartite graph. This aggregates the data using a distance-weighted average. We project both the ground truth and the predicted interactabilities following this procedure and present the results in Figure 4.

From this illustration, it is evident that our model identifies binding sites on proteins. There are observable errors, such as misidentified residues on the lower part of 2jbr. However, we emphasize that given the pairwise formulation of the task, these inaccurately labeled residues may exhibit complementarity to one of the partner’s interface residues.

3.5.2. ABLATION STUDY

Finally, we examine the impact of different design choices on our tasks. We already introduced in the methods three scenarios: `parallel`, `sequential` and `bipartite`. As mentioned above, the proposed mixed scenario `HoloProt` (Somnath et al., 2021) falls into the *sequential* framework with just one encoding block. Hence, we add this setting in our benchmark - with an enhanced protein encoder since we replace MeshCNN (Hanocka et al., 2019) with DiffusionNet - and refer to it as `holo`.

Another major design choice is the choice of the Message Passing (MP) component. We explore the use of three possible message-passing networks. Motivated by the success of DGCNN (Wang et al., 2019), in our `Att.` setting, we discard the geometric notion of a neighborhood, allowing for potentially long-distance message passing. In this setting, all nodes from the graphs attend to all vertices from the surface. To deal with the incurred computational burden, we use the recent memory-efficient Flash Attention (Dao et al., 2022). We also explore the use of more conventional Graph Convolutional Networks (GCN setting) (Kipf & Welling, 2016) and the use of Graph Attention networks (Veličković et al., 2017; Brody et al., 2021) for our final `GAT` setting. Finally, we also try using three or four blocks in our networks, always adjusting the network width to keep the number of parameters constant. Our results are presented in Table 3.

Both the `sequential` and `parallel` strategies display underwhelming results. This is explained in part by

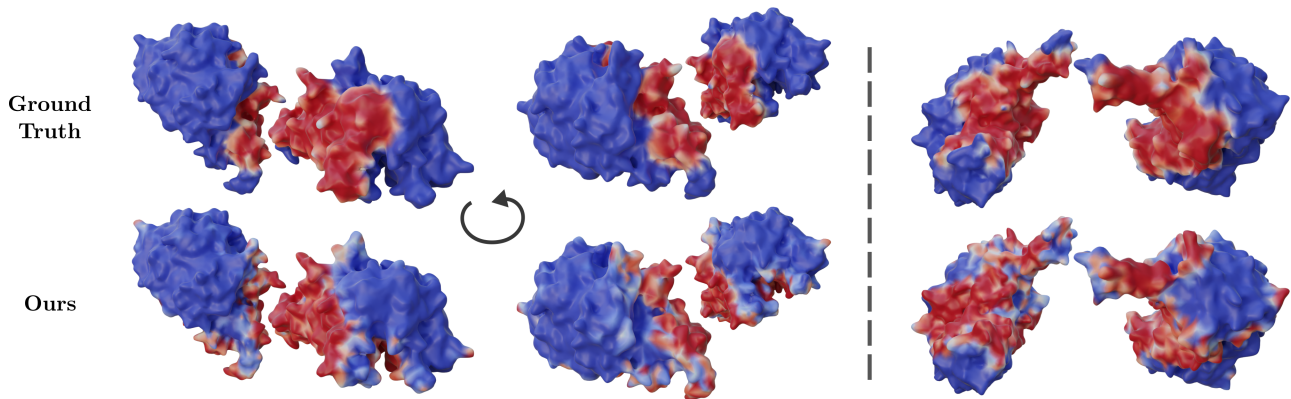


Figure 4: A qualitative view of our results. The top row is the ground truth with interaction sites in red. The bottom row displays our prediction. The two leftmost columns show the chains C and D of the protein with PDB id 2jbr under two rotated views of 180°. On the right, the interaction between chains A and B of the system with PDB id 2ono is shown.

Method	MP	Depth	MSP	PIP	PSR	
			AuROC	AuROC	local R	global R
parallel	-	-	0.550	0.5	0.390	0.777
sequential	-	-	0.609	0.855	0.319	0.71
holo	-	-	0.537	0.824	0.383	0.715
bipartite	Att.	3	0.689	0.792	0.400	0.792
	-	4	0.648	0.793	0.388	0.799
	GCN	3	0.626	0.858	0.420	0.800
	-	4	0.697	0.868	0.421	0.797
	GAT	3	0.707	0.859	0.434	0.833
	-	4	0.646	0.876	0.452	0.831

Table 3: Ablation study of our method. We compare different architecture designs, message-passing methods, and depths on our task. A detailed explanation of the different settings is available in the text.

their challenging optimization, with the employed message-passing likely being the root cause for this instability. Similarly, `holo` does not display a top performance, suggesting that the results in their paper could be enhanced by using the better-performing mixing strategies.

Among the `bipartite` settings, `Att.` is consistently outperformed by the localized message passing networks, except the MSP task where one network has a good performance. The other scenarios give an overall close performance, with an edge for the `GAT` network, and more particularly the deeper one. This is especially true for the PSR task, where the surface methods alone were failing. As hypothesized above, the mixed approach could simply use the surface as a way to diffuse information efficiently and at a long distance. This could explain why in this scenario, an attentive mechanism results in a performance boost.

4. Conclusion & Limitations

This study investigated the utility of the surface representation in machine learning on protein structures, comparing it against other methods on three `Atom3d` benchmark tasks. Although promising, surface methods alone did not achieve top-tier results, highlighting the need for ongoing innovation in this field. In contrast, the integration of surface and graph representations within our novel architecture led to substantial improvements, achieving state-of-the-art results across all benchmark tasks. Our ablation studies further indicated that simplistic approaches to combining different representations could lead to suboptimal performance. Beyond benchmark validation, our method’s application in identifying ligand-binding preferences set a new performance standard for this task.

Leveraging multiple representations with unique strengths seems to be a promising strategy for advancing protein anal-

ysis. Future research will focus on extending these hybrid approaches to additional tasks within structural bioinformatics. One of the current limitations of our approach is its significant memory requirements, highlighting the need for more efficient computational pipelines to reduce the resource demands of surface-based methods, in line with suggestions by (Sverrisson et al., 2021). Exploring the synergy between surface representations and other learning modalities for protein structures, such as geometric graphs (Duval et al., 2023), presents another exciting avenue for future research.

5. Acknowledgements & Funding

V.M. is paid by DataIA and Sanofi. This work was performed using HPC resources from GENCI-IDRIS (Grant 2023-AD010613356). Parts of this work are supported by the ANR Chair AIGRETTE and the ERC Starting Grant No. 758800 (EXPROTEA).

References

- Aumentado-Armstrong, T. Latent molecular optimization for targeted therapeutic design. *arXiv preprint arXiv:1809.02032*, 2018.
- Berman, H. M. The protein data bank. *Nucleic Acids Research*, 28(1):235–242, January 2000. doi: 10.1093/nar/28.1.235. URL <https://doi.org/10.1093/nar/28.1.235>.
- Brody, S., Alon, U., and Yahav, E. How attentive are graph attention networks? *arXiv preprint arXiv:2105.14491*, 2021.
- Bronstein, M. M. and Kokkinos, I. Scale-invariant heat kernel signatures for non-rigid shape recognition. In *2010 IEEE Computer Society Conference on Computer Vision and Pattern Recognition*. IEEE, June 2010. doi: 10.1109/cvpr.2010.5539838. URL <http://dx.doi.org/10.1109/CVPR.2010.5539838>.
- Bronstein, M. M., Bruna, J., LeCun, Y., Szlam, A., and Vandergheynst, P. Geometric deep learning: going beyond euclidean data. *IEEE Signal Processing Magazine*, 34(4): 18–42, 2017.
- Bruna, J., Zaremba, W., Szlam, A., and LeCun, Y. Spectral networks and locally connected networks on graphs. *arXiv preprint arXiv:1312.6203*, 2013.
- Cohen, T. and Welling, M. Group equivariant convolutional networks. In *International conference on machine learning*, pp. 2990–2999. PMLR, 2016a.
- Cohen, T. S. and Welling, M. Steerable cnns. *arXiv preprint arXiv:1612.08498*, 2016b.
- Dao, T., Fu, D., Ermon, S., Rudra, A., and Ré, C. Flashattention: Fast and memory-efficient exact attention with io-awareness. *Advances in Neural Information Processing Systems*, 35:16344–16359, 2022.
- Duval, A., Mathis, S. V., Joshi, C. K., Schmidt, V., Miret, S., Malliaros, F. D., Cohen, T., Liò, P., Bengio, Y., and Bronstein, M. A hitchhiker’s guide to geometric gnns for 3d atomic systems. *arXiv preprint arXiv:2312.07511*, 2023.
- Fontana, P., Dong, Y., Pi, X., Tong, A. B., Hecksel, C. W., Wang, L., Fu, T.-M., Bustamante, C., and Wu, H. Structure of cytoplasmic ring of nuclear pore complex by integrative cryo-em and alphafold. *Science*, 376(6598): eabm9326, 2022.
- Gainza, P., Sverrisson, F., Monti, F., Rodola, E., Boscaini, D., Bronstein, M., and Correia, B. Deciphering interaction fingerprints from protein molecular surfaces using geometric deep learning. *Nature Methods*, 17(2):184–192, 2020a.
- Gainza, P., Sverrisson, F., Monti, F., Rodola, E., Boscaini, D., Bronstein, M., and Correia, B. Deciphering interaction fingerprints from protein molecular surfaces using geometric deep learning. *Nature Methods*, 17(2):184–192, 2020b.
- Garland, M. and Heckbert, P. S. Surface simplification using quadric error metrics. In *Proceedings of the 24th annual conference on Computer graphics and interactive techniques*, pp. 209–216, 1997.
- Hanocka, R., Hertz, A., Fish, N., Giryas, R., Fleishman, S., and Cohen-Or, D. Meshcnn: a network with an edge. *ACM Transactions on Graphics (ToG)*, 38(4):1–12, 2019.
- Hermosilla, P., Schäfer, M., Lang, M., Fackelmann, G., Vázquez, P. P., Kozlíková, B., Krone, M., Ritschel, T., and Ropinski, T. Intrinsic-extrinsic convolution and pooling for learning on 3d protein structures. *arXiv preprint arXiv:2007.06252*, 2020.
- Ioffe, S. and Szegedy, C. Batch normalization: Accelerating deep network training by reducing internal covariate shift. In Bach, F. R. and Blei, D. M. (eds.), *Proceedings of the 32nd International Conference on Machine Learning, ICML 2015, Lille, France, 6-11 July 2015*, volume 37 of *JMLR Workshop and Conference Proceedings*, pp. 448–456. JMLR.org, 2015. URL <http://proceedings.mlr.press/v37/lofffe15.html>.
- Isert, C., Atz, K., and Schneider, G. Structure-based drug design with geometric deep learning. *Current Opinion in Structural Biology*, 79:102548, 2023.

- Jiménez, J., Doerr, S., Martínez-Rosell, G., Rose, A. S., and De Fabritiis, G. DeepSite: protein-binding site predictor using 3d-convolutional neural networks. *Bioinformatics*, 33(19):3036–3042, 2017.
- Jumper, J., Evans, R., Pritzel, A., Green, T., Figurnov, M., Ronneberger, O., Tunyasuvunakool, K., Bates, R., Žídek, A., Potapenko, A., et al. Highly accurate protein structure prediction with alphafold. *Nature*, 596(7873):583–589, 2021.
- Kipf, T. N. and Welling, M. Semi-supervised classification with graph convolutional networks. *arXiv preprint arXiv:1609.02907*, 2016.
- Kryshtafovych, A., Schwede, T., Topf, M., Fidelis, K., and Moulton, J. Critical assessment of methods of protein structure prediction (casp)—round xiii. *Proteins: Structure, Function, and Bioinformatics*, 87(12):1011–1020, 2019.
- Li, Q., Han, Z., and Wu, X.-M. Deeper insights into graph convolutional networks for semi-supervised learning. In *Proceedings of the AAAI conference on artificial intelligence*, volume 32, 2018.
- Lin, Z., Akin, H., Rao, R., Hie, B., Zhu, Z., Lu, W., Smetanin, N., Verkuil, R., Kabeli, O., Shmueli, Y., dos Santos Costa, A., Fazel-Zarandi, M., Sercu, T., Candido, S., and Rives, A. Evolutionary-scale prediction of atomic level protein structure with a language model. *bioRxiv*, 2022. URL <https://doi.org/10.1101/2022.07.20.500902>. bioRxiv 2022.07.20.500902.
- Masci, J., Boscaini, D., Bronstein, M., and Vandergheynst, P. Geodesic convolutional neural networks on riemannian manifolds. In *Proceedings of the IEEE international conference on computer vision workshops*, pp. 37–45, 2015.
- Meyer, M., Desbrun, M., Schröder, P., and Barr, A. H. Discrete differential-geometry operators for triangulated 2-manifolds. In *Visualization and mathematics III*, pp. 35–57. Springer, 2003.
- Monti, F., Boscaini, D., Masci, J., Rodola, E., Svoboda, J., and Bronstein, M. M. Geometric deep learning on graphs and manifolds using mixture model cnns. In *Proceedings of the IEEE conference on computer vision and pattern recognition*, pp. 5115–5124, 2017.
- Qi, C. R., Su, H., Mo, K., and Guibas, L. J. Pointnet: Deep learning on point sets for 3d classification and segmentation. In *Proceedings of the IEEE conference on computer vision and pattern recognition*, pp. 652–660, 2017.
- Rao, R. M., Liu, J., Verkuil, R., Meier, J., Canny, J., Abbeel, P., Sercu, T., and Rives, A. Msa transformer. In *International Conference on Machine Learning*, pp. 8844–8856. PMLR, 2021.
- Sanner, M. F., Olson, A. J., and Spehner, J.-C. Reduced surface: an efficient way to compute molecular surfaces. *Biopolymers*, 38(3):305–320, 1996.
- Sharp, N., Attaiki, S., Crane, K., and Ovsjanikov, M. Diffusionnet: Discretization agnostic learning on surfaces. *ACM Transactions on Graphics (TOG)*, 41(3):1–16, 2022.
- Somnath, V. R., Bunne, C., and Krause, A. Multi-scale representation learning on proteins. *Advances in Neural Information Processing Systems*, 34:25244–25255, 2021.
- Stärk, H., Ganea, O., Pattanaik, L., Barzilay, R., and Jaakkola, T. Equibind: Geometric deep learning for drug binding structure prediction. In *International conference on machine learning*, pp. 20503–20521. PMLR, 2022.
- Sun, J., Ovsjanikov, M., and Guibas, L. A concise and provably informative multi-scale signature based on heat diffusion. In *Computer graphics forum*, pp. 1383–1392. Wiley Online Library, 2009.
- Sverrisson, F., Feydy, J., Correia, B. E., and Bronstein, M. M. Fast end-to-end learning on protein surfaces. In *Proceedings of the IEEE/CVF Conference on Computer Vision and Pattern Recognition*, pp. 15272–15281, 2021.
- Townshend, R. J., Vögele, M., Suriana, P., Derry, A., Powers, A., Laloudakis, Y., Balachandar, S., Jing, B., Anderson, B., Eismann, S., et al. Atom3d: Tasks on molecules in three dimensions. *arXiv preprint arXiv:2012.04035*, 2020.
- Vallet, B. and Levy, B. Spectral Geometry Processing with Manifold Harmonics. *Computer Graphics Forum*, 2008. ISSN 1467-8659. doi: 10.1111/j.1467-8659.2008.01122.x.
- Veličković, P., Cucurull, G., Casanova, A., Romero, A., Lio, P., and Bengio, Y. Graph attention networks. *arXiv preprint arXiv:1710.10903*, 2017.
- Wang, Y., Sun, Y., Liu, Z., Sarma, S. E., Bronstein, M. M., and Solomon, J. M. Dynamic graph cnn for learning on point clouds. *ACM Transactions on Graphics (tog)*, 38(5):1–12, 2019.
- Wang, Y., Shen, Y., Chen, S., Wang, L., Ye, F., and Zhou, H. Learning harmonic molecular representations on riemannian manifold. *arXiv preprint arXiv:2303.15520*, 2023.
- Weiler, M., Geiger, M., Welling, M., Boomsma, W., and Cohen, T. S. 3d steerable cnns: Learning rotationally equivariant features in volumetric data. *Advances in Neural Information Processing Systems*, 31, 2018.

In this document, we compile all results and discussions that could not be included in the main manuscript due to page constraints.

More specifically, we first detail the specifics of our implementation in Appendix A. Following this, we provide a proof for Proposition 2.1 in Appendix B.

A. Implementation Details

The architecture we used is outlined in the main text. We employ our modified version of DiffusionNet (by adapting the original implementation provided by the authors¹) for each surface encoder and utilize GCN for the graph networks (using the implementation provided by PyTorch Geometric²). The surface methods were trained using only the surface encoder, whereas the mixed methods incorporated an additional graph encoder and a message-passing framework. When employing both encoders, we ensure the number of channels is equal for both. Thus, the variables are the number of "blocks" and the number of channels for each block. Our networks were trained in accordance with the parameter counts of other methods, strictly adhering to their optimization protocols, including the number of epochs, learning rate, and batch size.

For the surface methods, we consistently used 3 blocks, with 94, 90, and 96 channels for the PIP, MSP, and PSR tasks, respectively. For the bipartite methods, on the PIP task, we utilized 4 blocks with a width of 118; for MSP, 3 blocks with a width of 148; and for PSR, 4 blocks with a width of 160.

On the binding site classification task, our architecture featured 6 blocks, each with a width of 128.

B. Proof of Proposition 2.1

Proof. For simplicity we use the computations in the discrete setting (on meshes). Everything remains the same in the smooth (surface) setting, however. Let M_1 represent a shape modeled as a triangular mesh, with W_1 and A_1 denoting its cotangent Laplacian and area matrices, respectively. Therefore, its eigenvalue decomposition satisfies:

$$W_1 \phi^1 = \lambda^1 A_1 \phi^1.$$

Suppose M_2 is another mesh that is a scaled version of M_1 by a scaling factor a . Then, according to (Bronstein & Kokkinos, 2010):

$$\begin{aligned} A^2 &= a^2 A^1 \\ \lambda^2 &= \lambda^1 / a^2 \\ \phi^2 &= \phi^1 / a \end{aligned}$$

The heat kernel can be computed as per (Sun et al., 2009):

$$k_t(x, y) = \sum_i \exp(-\lambda_i t) \phi_i(x) \phi_i(y).$$

Consequently, we have:

$$\begin{aligned} k_t^2(x, y) &= \sum_i \exp(-\lambda_i^2 t) \phi_i^2(x) \phi_i^2(y) \\ &= \sum_i \exp(-\lambda_i^1 / a^2 t) \phi_i^1(x) \phi_i^1(y) / a^2 \\ &= k_{t/a^2}^1(x, y) / a^2 \end{aligned}$$

¹<https://github.com/nmwsharp/diffusion-net>

²<https://pytorch-geometric.readthedocs.io/en/latest/>

If $g(x, y)$ denotes the geodesic distance between two points on the surface x and y , then:

$$g^2(x, y) = ag^1(x, y).$$

Denoting $E.(t, x)$ as the *expected geodesic distance* of a Brownian motion starting from x after time t , we find:

$$\begin{aligned} E^2(t, x) &= \sum_y k_t^2(x, y) g^2(x, y) A^2(y) = \sum_y k_t^2(x, y) ag^1(x, y) a^2 A^1(y) \\ &= \sum_y k_t^2(x, y) ag^1(x, y) a^2 A^1(y) \\ &= \sum_y (k_{t/a^2}^1(x, y) / a^2) ag^1(x, y) a^2 A^1(y) \\ &= a \sum_y k_{t/a^2}^1(x, y) g^1(x, y) A^1(y) \\ &= aE^1(t/a^2, x). \end{aligned}$$

Interestingly, if we assume $E(t, x) = \sqrt{t}$ (as in the Euclidean setting), then: $aE^1(t/a^2, x) = a\sqrt{t/a^2} = \sqrt{t} = E^2(t, x)$. □

Based on this analysis, we proposed modifications to the *DiffusionNet* framework, leading to enhanced performance, as depicted in Figure 5.

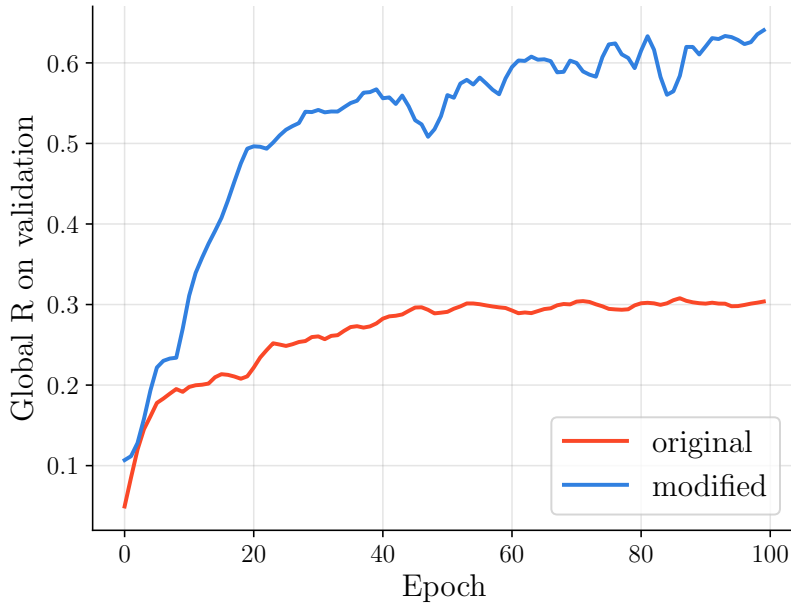


Figure 5: Changes in the global R curves before and after applying our enhancements to the *DiffusionNet* architecture. These adjustments significantly improve optimization, demonstrated by the improved convergence of the global R on the validation dataset for the PSR task.